Photoswitchable nanoparticles for in vivo cancer chemotherapy

Rong Tong[a,b], Homer H. Chiang[a], and Daniel S. Kohane[a,1]

[a]Laboratory for Biomaterials and Drug Delivery, Department of Anesthesiology, Division of Critical Care Medicine, Boston Children's Hospital, Harvard Medical School, Boston, MA 02115; and [b]Department of Chemical Engineering, Massachusetts Institute of Technology, Cambridge, MA 02139

Edited by Kristi S. Anseth, Howard Hughes Medical Institute, University of Colorado, Boulder, CO, and approved October 15, 2013 (received for review August 13, 2013)

There are many obstacles to effective cancer chemotherapy, including drug penetration and accumulation in tumors and drug systemic toxicity. The penetration of therapies into tumors is limited by the dense tumor matrix and by compression of the tumor vasculature. We have developed spiropyran-based nanoparticles that shrink from 103 to 49 nm upon irradiation at 365 nm. That shrinkage enhanced tissue penetration and drug release. Irradiation of s.c. HT-1080 tumors in nude mice administered i.v. docetaxel-containing nanoparticles was more effective treatment than free docetaxel or encapsulated docetaxel without irradiation. Irradiation at the tumor site also resulted in less systemic toxicity than if the nanoparticles were irradiated before injection, presumably because of less systemically distributed free drug. The enhanced efficacy of nanoparticles in irradiated tumors may have been related to the observed enhanced tumor penetration by nanoparticles and decompression of tumor blood vessels, which may also increase nanoparticle delivery into tumors.

nanomedicine | triggered drug delivery | photoswitching

Nanoparticles (NPs) have emerged as promising means to deliver a wide range of therapeutics for cancer treatment, as they can minimize systemic toxicity, improve drug circulation times, and enhance therapeutic effectiveness (1–4). NPs have the potential to preferentially deliver drugs to tumors, using the enhanced permeation and retention (EPR) effect (5), as new tumor vessels that sprout from existing vessels (6) are often leaky, with large pores (7, 8). However, the EPR effect is often compromised by the tumor microenvironment (9–11): compressed intratumoral blood and lymphatic vessels can hinder the delivery of blood-borne therapeutic agents (12, 13), while the dense collagen-rich extracellular matrix can retard the diffusion of nanomedicines within the tumor (14, 15). In addition, the proliferation of cancer cells is more rapid than that of capillary endothelial cells and can force vessels apart, reducing the vascular diameter and density in the tumor (16, 17). This increases the distance over which nanomedicines have to diffuse from blood vessels to target cells (>100 μm) (18). (In contrast, most cells in normal tissues are within a few micrometers of a blood vessel.) If drugs cannot be efficiently delivered to all cancer cells throughout the tumor, surviving tumor cells could repopulate and become resistant to both chemotherapy and radiotherapy (19). Overcoming physiological barriers to achieve uniform penetration remains a challenge in nanomedicine (20, 21).

We have recently developed a photoswitching nanoparticulate system that uses light as the means of remotely triggering a reversible change in particle volume that affects on-demand drug release and also enhances tissue penetration (22). Here, to enhance the NPs' performance in vivo, they have been modified so that drug release is minimal in the absence of light triggering, yet rapid upon irradiation. We have demonstrated the efficacy of such NPs in delivering docetaxel (Dtxl) both intratumorally (i.t.) and i.v. in a s.c. implanted fibrosarcoma (HT-1080 tumor) model, when triggered with UV light (365 nm). The biodistribution and intratumoral distribution, pharmacokinetics, and toxicity of the particles are examined.

Results

Light-Triggered Size Change and Dtxl Release. We have previously shown that hybrid NPs (NP_Hs; *SI Appendix*, Fig. S1) comprising spiropyran (SP) and lipid-polyethylene glycol (PEG) undergo a reversible volume change from 150 nm to 40 nm upon phototriggering (22). UV light (365 nm) induces hydrophobic SP to switch to zwitterionic merocyanine (MC; *SI Appendix*, Fig. S1*A*) (23), which alters the NP_H's physical assembly properties with an accompanying decrease in volume. Because MC is less stable than SP, MC NP_H will spontaneously revert to SP NP_H in darkness or under visible light, with an increase in NP size. Such reversible photoswitching of SP NP_H can enable repeated dosing from a single administration, and illumination enhances tissue penetration ex vivo.

Drug release in the absence of light triggering (i.e., in the off state) was minimized by increasing the hydrophobic interaction among lipids and SP by the introduction of cholesterol, which interacts strongly with phospholipids in liposomes to reduce bilayer permeability (24). NP_{HC}s (NP_Hs with cholesterol) were obtained by sonication of 1 wt% cholesterol with SP and lipid-PEG, and had an average hydrodynamic diameter of 103.5 ± 4.1 nm and a polydispersity of 0.03 ± 0.01. After UV illumination (1 W/cm^2, 35 s, ∼100% conversion to MC), MC NP_{HC} size decreased to 49.2 ± 3.3 nm (polydispersity of 0.05 ± 0.02, n = 5; Fig. 1*A*). NP_{HC}s with adjustable loadings of Dtxl (Dtxl/SP NP_{HC}s) up to 12.6 wt% and low polydispersities were readily obtained with sizes and photoswitching capabilities similar to those of NP_H (*SI Appendix*, Table S1).

In the absence of UV light triggering, Dtxl was released slowly from SP NP_{HC} in PBS (Fig. 1*B*). Upon UV irradiation (10 s), NP_{HC}s (Dtxl wt% = 9.4%) released 16.1% of the loaded Dtxl within 1 h as determined by HPLC, whereas less than 5% was released in the same period without UV irradiation (Fig. 1*B*). UV light triggering (10 s) conducted every 12 h for three cycles caused repeated increases in release at each event (n = 5; Fig. 1*B*).

Significance

The importance of this research is in the demonstration of the effectiveness and improved safety of a nanoparticulate chemotherapeutic formulation that can be phototriggered to shrink in size at the tumor site. That shrinkage enhanced nanoparticle penetration into tumors and also triggered local drug release. The result was increased efficacy and reduced systemic toxicity. The phototriggered formulation also relieved the compression of tumor blood vessels, which is a recognized barrier to nanoparticle accumulation in tumors.

Author contributions: R.T. and D.S.K. designed research; R.T. and H.H.C. performed research; R.T. and D.S.K. analyzed data; and R.T. and D.S.K. wrote the paper.

The authors declare no conflict of interest.

This article is a PNAS Direct Submission.

Freely available online through the PNAS open access option.

[1]To whom correspondence should be addressed. E-mail: daniel.kohane@childrens.harvard.edu.

This article contains supporting information online at www.pnas.org/lookup/suppl/doi:10.1073/pnas.1315336110/-/DCSupplemental.

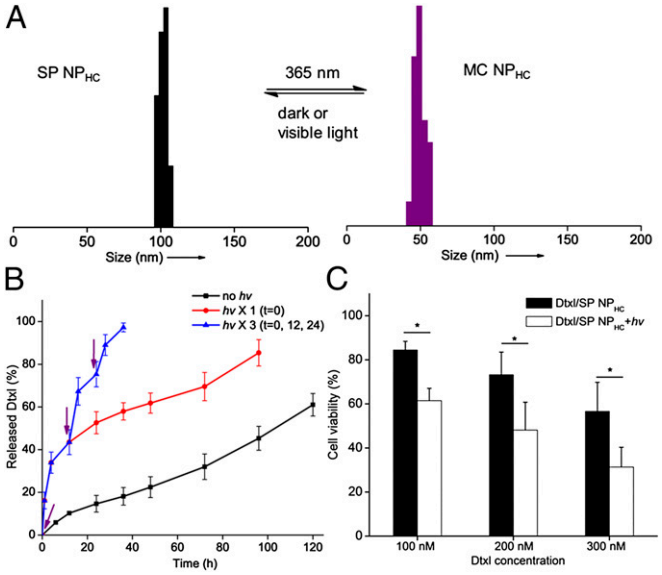

Fig. 1. In vitro characterization of photoswitching SP NP$_{HC}$s. (*A*) Dynamic light-scattering measurement of size changes of SP NP$_{HC}$s upon alternating UV (35 s) and visible light illumination (500–600 nm, 5 min, 0.5 W/cm^2). (*B*) Release of Dtxl from SP NP$_{HC}$ in the absence of irradiation; with UV irradiation for 10 s at t = 0 or with repeated UV irradiation at t = 0, 12, and 24 h. The times of irradiation are indicated by purple arrows ($n = 5$). (*C*) Effect of Dtxl/SP NP$_{HC}$ on HT-1080 cell viability, by MTT assay. Cells were incubated with NP$_{HC}$ for 4 h, washed with NP-free media, irradiated (10 s, 1 W/cm^2), and further incubated for a total time of 24 h. Data are means ± SD, $n = 6$; asterisks indicate $P < 0.005$. Dtxl, docetaxel; hν, UV irradiation; NP$_{HC}$, hybrid NPs with cholesterol; SP, spiropyran.

Light-triggered drug release increased the cytotoxicity of Dtxl/SP NP$_{HC}$ in HT-1080 cells. Cells were incubated with Dtxl/SP NP$_{HC}$s for 4 h, then washed and incubated in media without NP$_{HC}$s, irradiated (10 s), and further incubated for a total of 24 h. [We have previously found that SP NP$_H$ could be internalized by HeLa cells within 2 h (22).] Cell viability was then measured with an (3-(4,5-dimethylthiazol-2-yl)-2,5-diphenyltetrazolium bromide (MTT) assay (25). Light-triggered Dtxl/SP NP$_{HC}$s were more cytotoxic than Dtxl/SP NP$_{HC}$s without light triggering ($n = 6$, $P < 0.005$; Fig. 1*C*), presumably due to UV-triggered rapid intracellular release of Dtxl (22). SP NP$_{HC}$s themselves (no drug), with or without UV irradiation (10 s), did not cause significant cytotoxicity in HT-1080 cells except at extremely high concentrations (*SI Appendix*, Fig. S2).

We verified that the cholesterol-modified SP NP$_{HC}$s retained the light-triggered enhancement of diffusion that we had reported for NP$_H$ (22) by measuring diffusion through a well-established one-dimensional collagen gel model (26) with the same collagen concentration as in the matrix of 6–8-mm-diameter HT-1080 tumors [3.72 ± 0.63 mg/g tumor ($n = 5$) determined by a colorimetric hydroxyproline assay]. SP NP$_{HC}$s (1 mg/mL) containing the dye Cy5 (1 wt%) penetrated 6.7 ± 0.2 mm within 8 h at 37 °C without UV triggering; when triggered by UV for 10 s, they penetrated 10.5 ± 0.3 mm (56% further; $n = 4$, $P < 0.005$). [The mechanical properties of collagen are essentially unchanged by 1 h irradiation at 254 nm UV light at 15.8 J/cm^2 (27).]

UV Irradiation ex Vivo. We investigated the irradiation time required to trigger photoswitchable NP$_{HC}$s through the skin. The absorbance at 365 nm of mouse skin [from 6 to 8 wk *nu/nu* (nude) mice] was 0.758 ± 0.068 ($n = 4$)—that is, ~17% of light at 365 nm was transmitted (*SI Appendix*, Fig. S3*A*, black curve). Light absorption of skin above s.c. HT-1080 tumors was similar (*SI Appendix*, Fig. S3*A*, red curve). SP NP$_{HC}$s exhibited rapid photoswitching kinetics (half-time 14.8 s, same as described for NP$_H$) (22); through skin, the half-time was 25.9 s at a UV intensity of 1 W/cm^2 (*SI Appendix*, Fig. S3*B*). The half-time of the conversion from MC NP$_{HC}$ to SP NP$_{HC}$ is 2,741 ± 27 s in vitro. This suggests that the triggered NPs would remain as MC NP$_{HC}$s (i.e., reduced in size) for a few hours, during which they would penetrate tumors.

Intratumoral Injection of NP$_{HC}$s. As a preliminary to studies of i.v. administered SP NP$_{HC}$s, we examined their intratumoral distribution and effectiveness when delivered by direct injection at the tumor site. [Perforce this entailed NP deposition at the periphery of the tumors due to the difficulty of injecting into the high pressure deep in the tumor (28).] SP NP$_{HC}$s containing the fluorescent dye Cy5 (1 mg/kg) were injected into s.c. HT-1080 tumors (diameters ~6–8 mm), with or without immediately subsequent light triggering (15 s, 1 W/cm^2). Frozen sections of tumors collected 12 h postinjection revealed that the fluorescence of Cy5/SP NP$_{HC}$s was restricted to the injection site in the absence of light triggering, whereas light-triggered (365 nm, 15 s) NP$_{HC}$s were more broadly distributed (Fig. 2 *A* and *B*), as quantified by percentage of tumor area positive for Cy5 fluorescence (Fig. 2*C*; $n = 4$, $P < 0.001$). It is unlikely that the brief irradiation itself (15 J/cm^2) altered the tumor vasculature; for UV light over 320 nm, the dose to cause erythema in mice skin is ~3,000 J/cm^2 (29–31). Therefore, the increased distribution of fluorescence after irradiation was likely due to enhanced diffusive movement of NP$_{HC}$s.

We evaluated the efficacy of Dtxl/SP NP$_{HC}$ in s.c. implanted HT-1080 tumors in *nu/nu* mice, once those tumors reached ca. 100 mm^3 in size. The following treatments were administered as a single intratumoral injection ($n = 5$): (*i*) PBS, (*ii*) PBS with irradiation (365 nm, 10 s, 1 W/cm^2), (*iii*) Dtxl/SP NP$_{HC}$ (Dtxl 10 mg/kg), and (*iv*) Dtxl/SP NP$_{HC}$ with irradiation (10 s, 1 W/cm^2) (Fig. 2 *C* and *D*). Single intratumoral administrations of Dtxl/SP NP$_{HC}$ were efficacious in tumor reduction, with and without light triggering (Fig. 2*D*). Of note, two of five mice in the Dtxl/SP

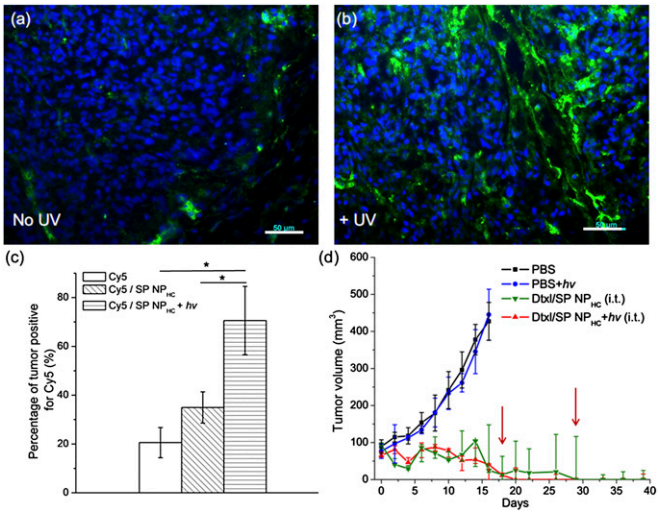

Fig. 2. Intratumoral distribution and efficacy of i.t. injected SP NP$_{HC}$s in animals with s.c. HT-1080 tumors. (*A* and *B*) Cy5/SP NP$_{HC}$s (Cy5 dose, 1 mg/kg) were injected i.t., then the tumors were either (*A*) not treated or (*B*) irradiated for 15 s at 365 nm, and excised for immunofluorescence imaging 12 h post-injection. Blue, cell nuclei stained by DAPI; green, Cy5/SP NP$_{HC}$. (Scale bar, 50 μm.) (*C*) Quantification of the percentage of tumor area positive for Cy5 ($n = 4$, with four sections from four tumors). Asterisks indicate $P < 0.005$. (*D*) In vivo efficacy of Dtxl/SP NP$_{HC}$ (Dtxl dose: 10 mg/kg, $n = 5$) given i.t. to s.c. HT-1080 tumors, without or with light triggering (15 s, 1 W/cm^2). Two of five mice in the Dtxl/SP NP$_{HC}$ group (green line) were euthanized as their tumor size exceeded 500 mm^3 (tumor diameter over 1 cm) on day 18 and 29 (red arrows). Data are medians ± quartiles.

NP_{HC} group had to be euthanized per animal protocol, as their tumor volumes exceeded 500 mm^3 (~1 cm diameter) on days 18 and 29 (*SI Appendix*, Fig. S4*A*). In contrast, all mice treated with Dtxl/SP NP_{HC}s and irradiation showed significant tumor reduction. In the groups administered PBS only (without and with light triggering), the tumors in all animals grew within 2 wk to the point where euthanasia was indicated. Animals treated with Dtxl/SP NP_{HC} did not show appreciable changes in body weight over 15 d, suggesting no severe systemic toxicity (*SI Appendix*, Fig. S4*B*).

Toxicity of Systemically Administered NP_{HC}s. Animals were given a single i.v. bolus of SP NP_{HC}s in *nu/nu* mice with 4–5-mm-diameter s.c. tumors at a high dosage of 400 mg/kg. Particles were drug free or contained Dtxl (40 mg/kg; dosage based on reported maximum tolerated dosage) (32). The tumor sites were irradiated (1 W/cm^2 for 20 s) or not in animals receiving SP NP_{HC}s containing Dtxl. Mice remained healthy during an observation period of 2 wk, without behavior changes or severe weight loss (<10%). Blood tests suggested that the hepatic function of the mice was normal (for alkaline phosphatase and alanine transferase, $P > 0.1$ for the comparison between mice treated with PBS and Dtxl/SP NP_{HC}s with irradiation; *SI Appendix*, Fig. S5). Red blood cell counts and characteristics were also not affected by the large dose of SP NP_{HC}s ($P > 0.2$ between mice treated with PBS and Dtxl/SP NP_{HC}s with irradiation; *SI Appendix*, Fig. S6). White blood cell counts were also not affected ($P > 0.2$ between mice treated with PBS and Dtxl/SP NP_{HC}s with irradiation) and platelet counts were not depressed (*SI Appendix*, Fig. S7). Hematoxylin-eosin–stained histological sections of organs harvested 72 h postinjection were normal (*SI Appendix*, Fig. S8).

Photoswitching Enhances Efficacy of Dtxl NP_{HC}s. We evaluated the efficacy of i.v.-injected Dtxl/SP NP_{HC} in s.c. HT-1080 tumors (Fig. 3 *A* and *B*; *SI Appendix*, Table S2). After tumors reached 100–150 mm^3 in volume, mice were treated with the following regimens ($n = 5$): (*i*) PBS, (*ii*) Dtxl, (*iii*) Dtxl/SP NP_{HC}, (*iv*) Dtxl/SP NP_{HC} converted to Dtxl/MC NP_{HC} by irradiation just before injection ("preirradiation"), or (*v*) Dtxl/SP NP_{HC} with irradiation (20 s, 1 W/cm^2) onto the tumor site 30 min postinjection ("postirradiation"; see *SI Appendix*, *Methods S6* for the rationales for irradiation times). The Dtxl dosing was 40 mg/kg. Mice treated with free Dtxl experienced severe weight loss (over 20%) within 4 d; significant body weight loss at day 6 was also seen in the group treated with Dtxl/MC NP_{HC} (preirradiation group, *SI Appendix*, Fig. S4*C*), presumably due to the considerable free Dtxl released from MC NP_{HC} upon irradiation (16.1% Dtxl was released in vitro within 1 h; Fig. 1*B*).

In the group treated with PBS, tumor volume rapidly exceeded 500 mm^3 (ca. tumor diameter over 1 cm) with a median tumor volume doubling time of 2.98 d. In contrast, in mice dosed with Dtxl/SP NP_{HC} the median tumor volume doubling time increased to 7.55 d (*SI Appendix*, Table S2), and all tumors reached 500 mm^3 (ca., tumor diameter over 1 cm) within 20 d. Irradiation of Dtxl/SP NP_{HC} at the tumor site (postirradiation) greatly improved efficacy: three of five mice survived over 100 d, with two mice having complete tumor resolution (comparison of survival curves for Dtxl/SP NP_{HC} groups with and without irradiation, by log-rank test, $P = 0.004$).

Triggering at the tumor site affected the efficacy and toxicity of Dtxl/SP NP_{HC}. The mouse body weights in the preirradiation group were lower than in postirradiated animals at day 12 ($P = 0.04$; *SI Appendix*, Fig. S4*C*). All animals in the preirradiation group were euthanized by day 75 due to tumor growth over 500 mm^3 (vs. three survivors to 100 d in postirradiated animals). The median tumor volume on day 53 in the preirradiation group was 163.8 mm^3 (two animals) versus 28.8 mm^3 in postirradiated animals (three animals). However, the difference between survival curves of preirradiation and postirradiation groups was not statistically significant ($P = 0.093$ by log-rank test). The differences between the in vivo results in preirradiation and postirradiation groups likely reflected the fact that in the preirradiation group, more free drug was released systemically, whereas in postirradiated animals, more Dtxl was released in the tumor.

Histological studies (*SI Appendix*, Fig. S9) showed that 96 h postinjection live tumor cells in the light-triggered Dtxl/SP NP_{HC} group were significantly decreased (tumor cell density decreased

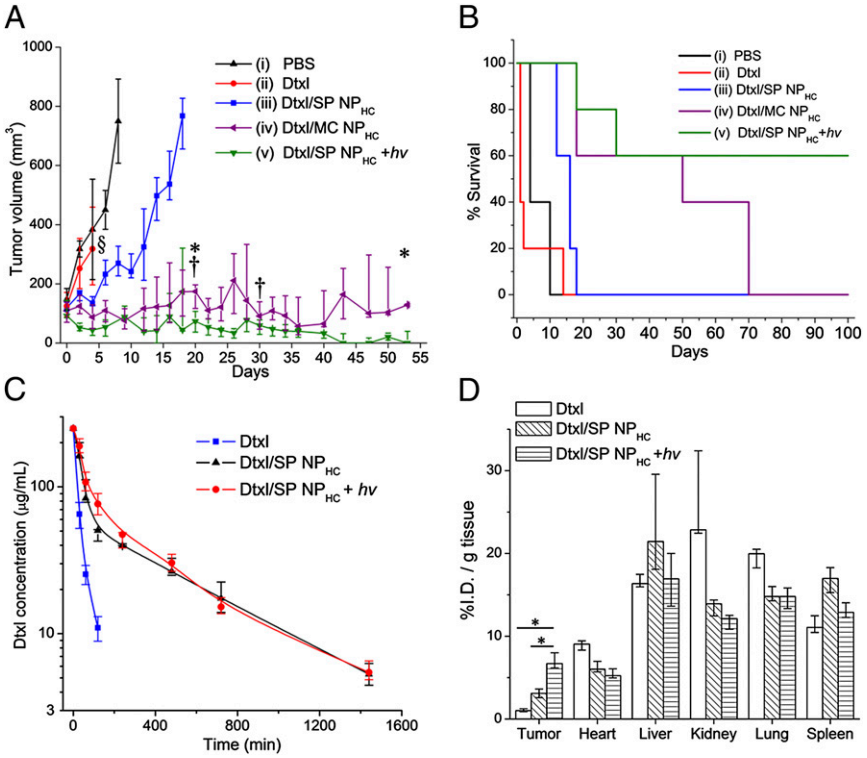

Fig. 3. Efficacy, pharmacokinetics, and biodistribution of i.v.-injected formulations in animals with s.c. HT-1080 tumors. (*A*) Effect on tumor growth inhibition (Dtxl dose: 40 mg/kg, $n = 5$). § indicates study termination for the group treated with Dtxl due to significant body weight loss (>20%). Mice with tumor volumes over 500 mm^3 were removed from the study (*, from the Dtxl/MC NP_{HC} group; †, from the Dtxl/SP NP_{HC} group with irradiation). (*B*) Kaplan–Meier plot for the same groups as in *A*. (*C*) Plasma concentration of Dtxl over time in mice after i.v. administration of Dtxl, Dtxl/SP NP_{HC}, and Dtxl/MC NP_{HC} (Dtxl dose: 10 mg/kg, $n = 5$). (*D*) Biodistribution of Dtxl, free or loaded in NP_{HC}s (with and without light triggering), in various tissues at 24 h after injection ($n = 5$). Results are expressed as a percentage of the total injected dose per tissue mass (%I.D./g). Data in *A*, *C*, and *D* are medians ± interquartile range. Asterisks indicate $P < 0.005$. Dtxl, docetaxel; *hν*, UV irradiation; NP_{HC}, hybrid NPs with cholesterol; SP, spiropyran.

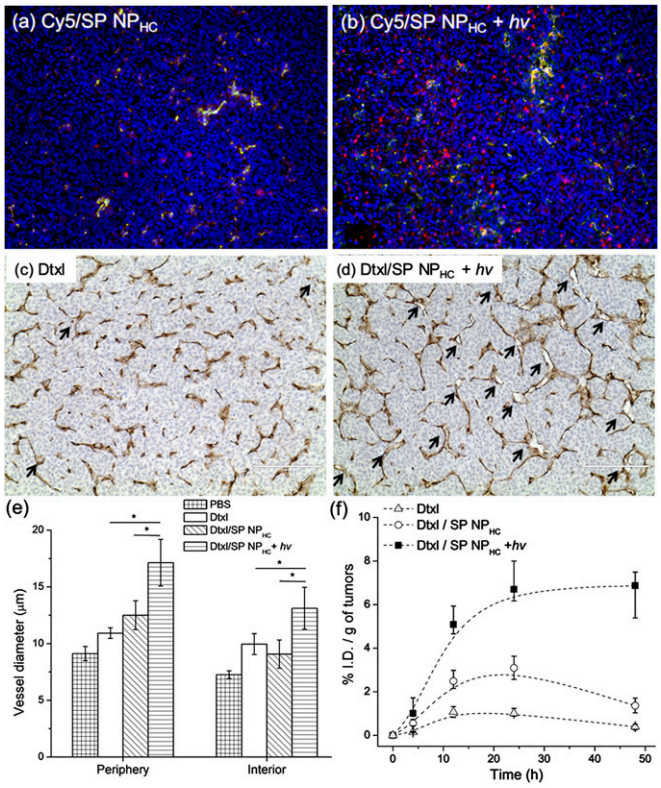

Fig. 4. Light triggering of SP NP$_{HC}$s enhanced particle diffusion and induced drug release to decompress vessels, leading to improved intratumoral accumulation of NP$_{HC}$s. (*A* and *B*) Representative images of intratumoral distribution of NPs 24 h after i.v. injection of Cy5/SP NP$_{HC}$s (red color) (*A*) without or (*B*) after light irradiation at tumor site (20 s, 1 W/cm^2, 30 min postinjection). Blue, cell nucleus; green, antibody against CD31 staining blood vessel endothelial cells; yellow, colocalization of red and green. (Scale bar, 100 μm.) (*C* and *D*) Representative immunohistology (of CD31) of tumor blood vessels 24 h after i.v. injection of (*C*) Dtxl, or (*D*) Dtxl/SP NP$_{HC}$s with irradiation of the tumor site under the same conditions as in *B*. Dtxl dose was 40 mg/kg in all groups. Vessel diameters were larger (indicated by arrows) in the irradiated group, as quantitated in *E*. (Scale bar, 200 μm.) In *E*, "periphery" refers to areas <1 mm away from the tumor edge, and "interior" to areas >1 mm inside tumors (*SI Appendix*, Fig. S13). Asterisk indicates $P < 0.01$. Data are means ± SD. (*F*) Intratumoral Dtxl accumulation over 24 h in animals treated with Dtxl, Dtxl/SP NP$_{HC}$s, and Dtxl/SP NP$_{HC}$s irradiated as in *D* ($n = 5$). Data are medians ± quartiles.

by 51.5% compared with the group treated with PBS, $P < 0.005$), whereas the groups treated with the same NP$_{HC}$s without light triggering or free Dtxl had decreases in cell density of 23.5% and 8.7%, respectively ($P = 0.05$ and 0.30 in comparison with the group treated with PBS, respectively).

NP Pharmacokinetics and Biodistribution. Because particle size has a marked impact on pharmacokinetics and biodistribution (33–36), we investigated whether light triggering at the tumor site would affect those parameters for Dtxl delivered by SP NP$_{HC}$s. The Dtxl concentration in blood plasma over time was fitted to a two-compartmental PK model. The mean elimination half-time ($t_{1/2\beta}$) of Dtxl/SP NP$_{HC}$, with or without light triggering (376 and 213 min, respectively; Fig. 3*C* and *SI Appendix*, Table S3), was significantly greater than that of free Dtxl (14 min, $P < 0.005$). The areas under the curves (AUCs) for Dtxl/SP NP$_{HC}$ without or with light triggering were both ~sixfold higher than the corresponding AUC for free Dtxl (*SI Appendix*, Table S3). Irradiation did not change the particle clearance rate ($P = 0.27$).

Biodistribution was studied by measuring the mean tissue concentration of Dtxl by HPLC in various organs 24 h after injection (Fig. 3*D*). The majority of Dtxl/SP NP$_{HC}$s accumulated in the liver and spleen, as is the case with many nanoparticulate systems (37, 38). The mean tumor uptake of Dtxl in light-triggered Dtxl/SP NP$_{HC}$ was 1.7-fold and 6.6-fold higher than those of nontriggered NP$_{HC}$ and free Dtxl, respectively ($P < 0.005$ for both).

Tumor Penetration by Phototriggered NPs. NP distribution within tumor tissues was investigated after injecting Cy5/SP NP$_{HC}$s i.v. and irradiating the tumor sites 30 min after administration (20 s, 1 W/cm^2). Tumor tissues were collected 24 h postinjection for immunofluorescent imaging of frozen sections. In the absence of irradiation, Cy5 fluorescence intensity remained largely localized to tumor vessels (demarcated by endothelial cells stained by anti-CD31), as indicated by the yellow color (colocalization of intratumoral vessels and Cy5/SP NP$_{HC}$s) in Fig. 4*A*, whereas Cy5 fluorescence was broadly distributed throughout the tumor tissue in irradiated mice (Fig. 4*B*). Quantitative analysis confirmed that the distribution of Cy5/SP NP$_{HC}$s was more diffuse throughout the tumor in irradiated animals, as seen in the increased percentage of tumor area positive for Cy5 fluorescence and the increased distance of extravasated NP$_{HC}$s from blood vessels (*SI Appendix*, Fig. S10).

Effect of Light-Triggered Intratumoral Drug Release and Enhanced Penetration on the Tumor Vasculature. We hypothesized that the increased tumor killing by photoswitching Dtxl/SP NP$_{HC}$s was due to tumor cell apoptosis and tumor vessel decompression resulting from light-triggered Dtxl release from NP$_{HC}$s. The vascular decompression would enhance NP delivery into tumors. Studies have shown that systemic administration of taxanes (paclitaxel or Dtxl) can decompress intratumoral collapsed blood vessels and increase tumor blood flow without a change in vessels numbers (39), improving the delivery of therapeutics and improving tumor response (40–44).

Treatment with Dtxl/SP NP$_{HC}$s irradiated at the tumor site increased apoptosis (assayed by TUNEL staining) and decreased tumor cell proliferation (assayed by ki67 staining) in HT-1080 tumors 24 h after injection, compared with other treatment groups (*SI Appendix*, Fig. S11*A*). Tumor vessel density was not affected in any treatment group (*SI Appendix*, Fig. S11*B*). To assess the effect of treatments on blood vessel size, we measured vessel diameters in the periphery and interior of HT-1080 tumors (Fig. 4 *C–E*; *SI Appendix*, Fig. S12). Vascular diameters were significantly increased at 24 h in the periphery of tumors treated with Dtxl/SP NP$_{HC}$s, with or without irradiation, whereas those diameters did not change significantly in the untreated and free Dtxl groups (Fig. 4 *C–E*; *SI Appendix*, Fig. S12). Importantly, vascular diameters were increased in the tumor interiors, and vessels had open lumens, in animals treated with Dtxl/SP NP$_{HC}$ with UV light irradiation (Fig. 4*E*, *SI Appendix*, Fig. S12), compared with those treated with free Dtxl or nontriggered particles (Fig. 4 *C* and *D*; *SI Appendix*, Fig. S12). In the single animal treated with light-triggered Dtxl/SP NP$_{HC}$s that was examined at 96 h, most tumor blood vessels had lumens over 15 μm (*SI Appendix*, Fig. S13).

To determine whether the increased vessel caliber affected blood perfusion, we identified perfused tumor vessels by staining with i.v. injected fluorescein–lectin (45–47). We calculated the percentage of all vessels (stained by anti-CD31) that were perfused (stained by fluorescein–lectin). At 24 and 48 h postinjection, Dtxl/SP NP$_{HC}$s with light irradiation significantly increased the percentage of perfused blood vessels, compared with groups treated with Dtxl/SP NP$_{HC}$ or free Dtxl (both $P < 0.01$; *SI Appendix*, Fig. S11*C*). These changes in the vasculature, along with the enhanced perfusion, suggest a decrease in intratumoral pressure (15, 20, 39, 48–51). The increased fraction of perfused blood vessels due to the decompression of blood vessels was associated with enhanced intratumoral accumulation of NP$_{HC}$s: Dtxl delivered by Dtxl/SP NP$_{HC}$s with irradiation led to intratumoral accumulation of 6% of the injected dose per gram

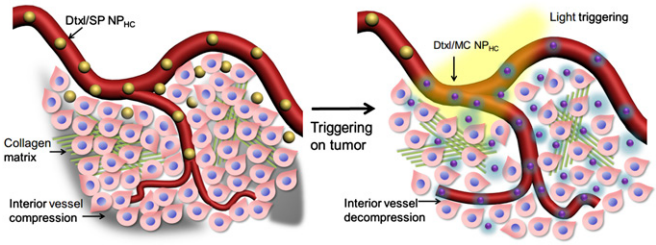

Fig. 5. Effects of light triggering of Dtxl/SP NP$_{HC}$s (yellow spheres) in the tumor vasculature. The dense collagen matrix (green lines) and compressed vessels prevent unshrunken NP$_{HC}$s from delivering drugs within the tumor (gray region). Tumor irradiation shrinks NP$_{HC}$s (purple spheres), which enhances their penetration through the collagen matrix throughout the tumor. The triggered released of Dtxl (the cyan glow surrounding NP$_{HC}$s) kills tumor cells, which leads to dilation of compressed intratumoral blood vessels. The decompression of vessels facilitates the transport of NP$_{HC}$s into the tumor interior.

of tissue (%I.D./g) from 24 to 48 h, higher than with free Dtxl and nonirradiated NP$_{HC}$s ($P < 0.01$ for both; Fig. 4*F*).

Discussion

Light-triggered Dtxl/SP NP$_{HC}$ induced tumor cell death (*SI Appendix*, Fig. S11*A*) and increased intratumoral vessel diameters and tumor perfusion (Fig. 4*E*; *SI Appendix*, Fig. S11*C*). These effects, along with the particles' light-triggered ability to penetrate collagen matrices, enhanced the accumulation of NP$_{HC}$s through tumor tissues (Fig. 4*F*) and inhibited tumor growth (Fig. 3*A*), as schematized in Fig. 5. UV-triggered size change and drug release both affected drug accumulation in the tumor (the %I.D./g), by different mechanisms. Irradiation-induced size change enhanced particle penetration and hence the %I.D./g (Fig. 3*D*), but did not affect the tissue structure itself in the absence of drug release (*SI Appendix*, Fig. S11*B*). UV-triggered drug release led to vessel decompression to a greater extent than did nontriggered drug release (Fig. 4*E*). This vessel decompression, which was established by 24 h at the latest (Fig. 4 *C*–*E*), perhaps further facilitated the penetration of drug-containing particles (Fig. 4*F*).

It is possible that the portion of the effect of the triggered Dtxl/SP NP$_{HC}$s that is attributable to tumor penetration could be achieved by injecting NPs with the fixed smaller size of the posttriggered MC NP$_{HC}$s. However, those particles would not provide the beneficial effect of the triggered drug release within the tumor (Fig. 4*E*). A possible solution that would provide both enhanced penetration and triggered release would be to create triggerable particles that are formulated at the smaller size. A potential difficulty in that approach, however, is that most triggerable particles of that (or any) size (52, 53) tend to be depleted or destroyed by the single triggering event. Consequently, they would not be available after triggering to penetrate deeper into tissues and/or provide sustained drug release in situ—as would be the case with the formulation presented here. Moreover, this formulation has the potential for repeated triggering (Fig. 1*B*), although we did not study the antitumor effects of that capability in this report.

The wavelength used for triggering is of obvious importance. The wavelength at which SP is triggered could not be readily shifted to the near-infrared range as the covalent bond in SP requires a high-energy photon to break (54), and near-infrared light is relatively low in energy ($E = h\nu$). However, the photoswitching of SP NP$_{HC}$s could potentially be triggered at depths up to centimeters by using near-infrared lasers (55) [e.g., by two-photon technology with wavelength ~720 nm (56–59)]. The use of near-infrared light would allow deeper tissue penetration, including through soft tissues, bone, and intact skull (53, 55, 60, 61). UV light could potentially also be used deep within the body by use of fiber optics and endoscopy (60–62).

The safety of the wavelength used also is important. UV light is divided into UVA (320–400 nm) and UVB (280–320 nm). UVA light has been used clinically to treat various diseases, including some skin conditions (e.g., psoriasis, vitiligo, atopic dermatitis) (63–65) and corneal collagen cross-linking (66, 67). Brief irradiation with 365 nm light at low energy is not considered a risk for skin cancer (68, 69). It bears mentioning that the treatment of cancers routinely involves forms of radiation that are potentially much more harmful (i.e., radiation oncology).

Conclusion

We have demonstrated the in vivo efficacy of photoswitchable NP$_{HC}$s in a s.c. implanted tumor model. There have been a small number of strategies to enhance tumor penetration (21, 33–36, 48, 70–75), including applying external energy (e.g., heat) to dilate vessels (76, 77), using tissue-penetration peptides (78–80), or degrading the stromal matrix by applying proteases (e.g., collagenase and relaxin) (81–84). Improved tumor penetration by nanotherapeutics can also be achieved by coadministration of agents that enhance tumor perfusion by decreasing tumor interstitial fluid pressure (e.g., by inhibitors of TGF-β) (85, 86). Light-triggering of Dtxl/SP NP$_{HC}$ increased NP diffusion through the tumor collagen matrix and induced release of Dtxl, which opened compressed intratumoral vessels by killing tumor cells. The resulting enhanced perfusion further increased the intratumoral penetration of NPs. Poor perfusion of tumor tissues is a recognized mechanical barrier to drug delivery (11, 87, 88); strategies like the one presented here may modify the tumor microenvironment to favor NPs' tumor penetration and distribution. The use of nanoparticulate triggering systems may also minimize systemic toxicity.

ACKNOWLEDGMENTS. We thank the histology core facility at Koch Institute and Comparative Pathology Lab at the Massachusetts Institute of Technology for their technical support. The work was supported by a grant from Sanofi-Aventis and the National Institutes of Health (R01 GM073626).

1. Langer R (1993) Polymer-controlled drug-delivery systems. *Acc Chem Res* 26(10):537–542.
2. Langer R, Folkman J (1976) Polymers for the sustained release of proteins and other macromolecules. *Nature* 263(5580):797–800.
3. Gref R, et al. (1994) Biodegradable long-circulating polymeric nanospheres. *Science* 263(5153):1600–1603.
4. Langer R (1998) Drug delivery and targeting. *Nature* 392(6679, Suppl):5–10.
5. Matsumura Y, Maeda H (1986) A new concept for macromolecular therapeutics in cancer chemotherapy: Mechanism of tumoritropic accumulation of proteins and the antitumor agent smancs. *Cancer Res* 46(12 Pt 1):6387–6392.
6. Carmeliet P, Jain RK (2011) Principles and mechanisms of vessel normalization for cancer and other angiogenic diseases. *Nat Rev Drug Discov* 10(6):417–427.
7. Yuan F, et al. (1995) Vascular permeability in a human tumor xenograft: Molecular size dependence and cutoff size. *Cancer Res* 55(17):3752–3756.
8. Yuan F, et al. (1996) Time-dependent vascular regression and permeability changes in established human tumor xenografts induced by an anti-vascular endothelial growth factor/vascular permeability factor antibody. *Proc Natl Acad Sci USA* 93(25):14765–14770.
9. Prabhakar U, et al. (2013) Challenges and key considerations of the enhanced permeability and retention effect for nanomedicine drug delivery in oncology. *Cancer Res* 73(8):2412–2417.
10. Jain RK (1998) Delivery of molecular and cellular medicine to solid tumors. *J Control Release* 53(1-3):49–67.
11. Jain RK (2001) Delivery of molecular and cellular medicine to solid tumors. *Adv Drug Deliv Rev* 46(1-3):149–168.
12. Leu AJ, Berk DA, Lymboussaki A, Alitalo K, Jain RK (2000) Absence of functional lymphatics within a murine sarcoma: A molecular and functional evaluation. *Cancer Res* 60(16):4324–4327.
13. Padera TP, et al. (2004) Pathology: Cancer cells compress intratumour vessels. *Nature* 427(6976):695.
14. Netti PA, Berk DA, Swartz MA, Grodzinsky AJ, Jain RK (2000) Role of extracellular matrix assembly in interstitial transport in solid tumors. *Cancer Res* 60(9):2497–2503.
15. Stylianopoulos T, et al. (2012) Causes, consequences, and remedies for growth-induced solid stress in murine and human tumors. *Proc Natl Acad Sci USA* 109(38):15101–15108.
16. Tannock IF (1968) The relation between cell proliferation and the vascular system in a transplanted mouse mammary tumour. *Br J Cancer* 22(2):258–273.
17. Denekamp J, Hobson B (1982) Endothelial-cell proliferation in experimental tumours. *Br J Cancer* 46(5):711–720.
18. Thomlinson RH, Gray LH (1955) The histological structure of some human lung cancers and the possible implications for radiotherapy. *Br J Cancer* 9(4):539–549.

19. Minchinton AI, Tannock IF (2006) Drug penetration in solid tumours. *Nat Rev Cancer* 6(8):583–592.
20. Jain RK, Stylianopoulos T (2010) Delivering nanomedicine to solid tumors. *Nat Rev Clin Oncol* 7(11):653–664.
21. Chauhan VP, Stylianopoulos T, Boucher Y, Jain RK (2011) Delivery of molecular and nanoscale medicine to tumors: Transport barriers and strategies. *Annu Rev Chem Biomol Eng* 2(1):281–298.
22. Tong R, Hemmati HD, Langer R, Kohane DS (2012) Photoswitchable nanoparticles for triggered tissue penetration and drug delivery. *J Am Chem Soc* 134(21):8848–8855.
23. Minkin VI (2004) Photo-, thermo-, solvato-, and electrochromic spiroheterocyclic compounds. *Chem Rev* 104(5):2751–2776.
24. Corvera E, Mouritsen OG, Singer MA, Zuckermann MJ (1992) The permeability and the effect of acyl-chain length for phospholipid bilayers containing cholesterol: Theory and experiment. *Biochim Biophys Acta* 1107(2):261–270.
25. Mosmann T (1983) Rapid colorimetric assay for cellular growth and survival: Application to proliferation and cytotoxicity assays. *J Immunol Methods* 65(1-2):55–63.
26. Ramanujan S, et al. (2002) Diffusion and convection in collagen gels: Implications for transport in the tumor interstitium. *Biophys J* 83(3):1650–1660.
27. Sionkowska A, Wess T (2004) Mechanical properties of UV irradiated rat tail tendon (RTT) collagen. *Int J Biol Macromol* 34(1-2):9–12.
28. Ohlfest JR, Ivics Z, Izsvák Z (2009) *Transposable Elements as Plasmid-Based Vectors for Long-Term Gene Transfer into Tumors. Gene Therapy of Cancer, Methods in Molecular Biology*, eds Walther W, Stein US (Humana Press, New York), Vol 542, pp 105–116.
29. Kligman LH (1989) The ultraviolet-irradiated hairless mouse: A model for photoaging. *J Am Acad Dermatol* 21(3 Pt 2):623–631.
30. Yano K, Oura H, Detmar M (2002) Targeted overexpression of the angiogenesis inhibitor thrombospondin-1 in the epidermis of transgenic mice prevents ultraviolet-B-induced angiogenesis and cutaneous photo-damage. *J Invest Dermatol* 118(5):800–805.
31. Sawane M, Kajiya K (2012) Ultraviolet light-induced changes of lymphatic and blood vasculature in skin and their molecular mechanisms. *Exp Dermatol* 21(Suppl 1):22–25.
32. Bissery MC, Nohynek G, Sanderink GJ, Lavelle F (1995) Docetaxel (Taxotere): A review of preclinical and clinical experience. Part I: Preclinical experience. *Anticancer Drugs* 6(3):339–355.
33. Perrault SD, Walkey C, Jennings T, Fischer HC, Chan WCW (2009) Mediating tumor targeting efficiency of nanoparticles through design. *Nano Lett* 9(5):1909–1915.
34. Lee H, Fonge H, Hoang B, Reilly RM, Allen C (2010) The effects of particle size and molecular targeting on the intratumoral and subcellular distribution of polymeric nanoparticles. *Mol Pharm* 7(4):1195–1208.
35. Tang L, Fan TM, Borst LB, Cheng J (2012) Synthesis and biological response of size-specific, monodisperse drug-silica nanoconjugates. *ACS Nano* 6(5):3954–3966.
36. Cabral H, et al. (2011) Accumulation of sub-100 nm polymeric micelles in poorly permeable tumours depends on size. *Nat Nanotechnol* 6(12):815–823.
37. Cheng J, et al. (2007) Formulation of functionalized PLGA-PEG nanoparticles for in vivo targeted drug delivery. *Biomaterials* 28(5):869–876.
38. Alexis F, Pridgen E, Molnar LK, Farokhzad OC (2008) Factors affecting the clearance and biodistribution of polymeric nanoparticles. *Mol Pharm* 5(4):505–515.
39. Griffon-Etienne G, Boucher Y, Brekken C, Suit HD, Jain RK (1999) Taxane-induced apoptosis decompresses blood vessels and lowers interstitial fluid pressure in solid tumors: Clinical implications. *Cancer Res* 59(15):3776–3782.
40. Mason KA, Hunter NR, Milas M, Abbruzzese JL, Milas L (1997) Docetaxel enhances tumor radioresponse in vivo. *Clin Cancer Res* 3(12):2431–2438.
41. Baselga J, Norton L, Albanell J, Kim YM, Mendelsohn J (1998) Recombinant humanized anti-HER2 antibody (Herceptin) enhances the antitumor activity of paclitaxel and doxorubicin against HER2/neu overexpressing human breast cancer xenografts. *Cancer Res* 58(13):2825–2831.
42. Holden SA, Lan Y, Pardo AM, Wesolowski JS, Gillies SD (2001) Augmentation of antitumor activity of an antibody-interleukin 2 immunocytokine with chemotherapeutic agents. *Clin Cancer Res* 7(9):2862–2869.
43. Lu D, Wientjes MG, Lu Z, Au JL-S (2007) Tumor priming enhances delivery and efficacy of nanomedicines. *J Pharmacol Exp Ther* 322(1):80–88.
44. Wong HL, Shen Z, Lu Z, Wientjes MG, Au JLS (2011) Paclitaxel tumor-priming enhances siRNA delivery and transfection in 3-dimensional tumor cultures. *Mol Pharm* 8(3):833–840.
45. Thurston G, Baluk P, Hirata A, McDonald DM (1996) Permeability-related changes revealed at endothelial cell borders in inflamed venules by lectin binding. *Am J Physiol* 271(6):H2547–H2562.
46. Hashizume H, et al. (2000) Openings between defective endothelial cells explain tumor vessel leakiness. *Am J Pathol* 156(4):1363–1380.
47. Chang YS, et al. (2000) Mosaic blood vessels in tumors: Frequency of cancer cells in contact with flowing blood. *Proc Natl Acad Sci USA* 97(26):14608–14613.
48. Chauhan VP, et al. (2012) Normalization of tumour blood vessels improves the delivery of nanomedicines in a size-dependent manner. *Nat Nanotechnol* 7(6):383–388.
49. Netti PA, et al. (1999) Enhancement of fluid filtration across tumor vessels: Implication for delivery of macromolecules. *Proc Natl Acad Sci USA* 96(6):3137–3142.
50. Yuan F, et al. (1994) Vascular permeability and microcirculation of gliomas and mammary carcinomas transplanted in rat and mouse cranial windows. *Cancer Res* 54(17):4564–4568.
51. Pluen A, et al. (2001) Role of tumor-host interactions in interstitial diffusion of macromolecules: Cranial vs. subcutaneous tumors. *Proc Natl Acad Sci USA* 98(8):4628–4633.
52. Timko BP, Dvir T, Kohane DS (2010) Remotely triggerable drug delivery systems. *Adv Mater* 22(44):4925–4943.
53. Tong R, Kohane DS (2012) Shedding light on nanomedicine. *Wiley Interdiscip Rev Nanomed Nanobiotechnol* 4(6):638–662.
54. Berkovic G, Krongauz V, Weiss V (2000) Spiropyrans and spirooxazines for memories and switches. *Chem Rev* 100(5):1741–1754.
55. Srinivasan S, et al. (2003) Interpreting hemoglobin and water concentration, oxygen saturation, and scattering measured in vivo by near-infrared breast tomography. *Proc Natl Acad Sci USA* 100(21):12349–12354.
56. Perry SW, Burke RM, Brown EB (2012) Two-photon and second harmonic microscopy in clinical and translational cancer research. *Ann Biomed Eng* 40(2):277–291.
57. Marriott G, et al. (2008) Optical lock-in detection imaging microscopy for contrast-enhanced imaging in living cells. *Proc Natl Acad Sci USA* 105(46):17789–17794.
58. Liu Q, Yang T, Feng W, Li F (2012) Blue-emissive upconversion nanoparticles for low-power-excited bioimaging in vivo. *J Am Chem Soc* 134(11):5390–5397.
59. Jayakumar MKG, Idris NM, Zhang Y (2012) Remote activation of biomolecules in deep tissues using near-infrared-to-UV upconversion nanotransducers. *Proc Natl Acad Sci USA* 109(22):8483–8488.
60. Weissleder R (2001) A clearer vision for in vivo imaging. *Nat Biotechnol* 19(4):316–317.
61. Yelin D, et al. (2006) Three-dimensional miniature endoscopy. *Nature* 443(7113):765.
62. Flusberg BA, et al. (2005) Fiber-optic fluorescence imaging. *Nat Methods* 2(12): 941–950.
63. Pathak MA, Fitzpatrick TB (1992) The evolution of photochemotherapy with psoralens and UVA (PUVA): 2000 BC to 1992 AD. *J Photochem Photobiol B* 14(1-2):3–22.
64. Njoo MD, Spuls PI, Bos JD, Westerhof W, Bossuyt PMM (1998) Nonsurgical repigmentation therapies in vitiligo. Meta-analysis of the literature. *Arch Dermatol* 134(12):1532–1540.
65. Bethea D, et al. (1999) Psoralen photobiology and photochemotherapy: 50 years of science and medicine. *J Dermatol Sci* 19(2):78–88.
66. Hafezi F, Kanellopoulos J, Wiltfang R, Seiler T (2007) Corneal collagen crosslinking with riboflavin and ultraviolet A to treat induced keratectasia after laser in situ keratomileusis. *J Cataract Refract Surg* 33(12):2035–2040.
67. Spoerl E, Mrochen M, Sliney D, Trokel S, Seiler T (2007) Safety of UVA-riboflavin cross-linking of the cornea. *Cornea* 26(4):385–389.
68. de Gruijl FR, et al. (1993) Wavelength dependence of skin cancer induction by ultraviolet irradiation of albino hairless mice. *Cancer Res* 53(1):53–60.
69. Bowden GT (2004) Prevention of non-melanoma skin cancer by targeting ultraviolet-B-light signalling. *Nat Rev Cancer* 4(1):23–35.
70. Jiang W, Kim BYS, Rutka JT, Chan WCW (2008) Nanoparticle-mediated cellular response is size-dependent. *Nat Nanotechnol* 3(3):145–150.
71. Popović Z, et al. (2010) A nanoparticle size series for in vivo fluorescence imaging. *Angew Chem Int Ed Engl* 49(46):8649–8652.
72. Perry JL, et al. (2012) PEGylated PRINT nanoparticles: The impact of PEG density on protein binding, macrophage association, biodistribution, and pharmacokinetics. *Nano Lett* 12(10):5304–5310.
73. Tang L, et al. (2012) Aptamer-functionalized, ultra-small, monodisperse silica nanoconjugates for targeted dual-modal imaging of lymph nodes with metastatic tumors. *Angew Chem Int Ed Engl* 51(51):12721–12726.
74. Choi CHJ, Alabi CA, Webster P, Davis ME (2010) Mechanism of active targeting in solid tumors with transferrin-containing gold nanoparticles. *Proc Natl Acad Sci USA* 107(3): 1235–1240.
75. Bartlett DW, Su H, Hildebrandt IJ, Weber WA, Davis ME (2007) Impact of tumor-specific targeting on the biodistribution and efficacy of siRNA nanoparticles measured by multimodality in vivo imaging. *Proc Natl Acad Sci USA* 104(39):15549–15554.
76. Kong G, Braun RD, Dewhirst MW (2000) Hyperthermia enables tumor-specific nanoparticle delivery: Effect of particle size. *Cancer Res* 60(16):4440–4445.
77. Ponce AM, et al. (2007) Magnetic resonance imaging of temperature-sensitive liposome release: Drug dose painting and antitumor effects. *J Natl Cancer Inst* 99(1):53–63.
78. Alberici L, et al. (2013) De novo design of a tumor-penetrating peptide. *Cancer Res* 73(2):804–812.
79. Sugahara KN, et al. (2010) Coadministration of a tumor-penetrating peptide enhances the efficacy of cancer drugs. *Science* 328(5981):1031–1035.
80. Ren Y, et al. (2012) Targeted tumor-penetrating siRNA nanocomplexes for credentialing the ovarian cancer oncogene ID4. *Sci Transl Med* 4(147):ra112.
81. McKee TD, et al. (2006) Degradation of fibrillar collagen in a human melanoma xenograft improves the efficacy of an oncolytic herpes simplex virus vector. *Cancer Res* 66(5):2509–2513.
82. Mok W, Boucher Y, Jain RK (2007) Matrix metalloproteinases-1 and -8 improve the distribution and efficacy of an oncolytic virus. *Cancer Res* 67(22):10664–10668.
83. Brown E, et al. (2003) Dynamic imaging of collagen and its modulation in tumors in vivo using second-harmonic generation. *Nat Med* 9(6):796–800.
84. Provenzano PP, et al. (2012) Enzymatic targeting of the stroma ablates physical barriers to treatment of pancreatic ductal adenocarcinoma. *Cancer Cell* 21(3):418–429.
85. Liu J, et al. (2012) TGF-β blockade improves the distribution and efficacy of therapeutics in breast carcinoma by normalizing the tumor stroma. *Proc Natl Acad Sci USA* 109(41):16618–16623.
86. Kano MR, et al. (2007) Improvement of cancer-targeting therapy, using nanocarriers for intractable solid tumors by inhibition of TGF-β signaling. *Proc Natl Acad Sci USA* 104(9):3460–3465.
87. Gillies RJ, Schornack PA, Secomb TW, Raghunand N (1999) Causes and effects of heterogeneous perfusion in tumors. *Neoplasia* 1(3):197–207.
88. Hamberg LM, Kristjansen PEG, Hunter GJ, Wolf GL, Jain RK (1994) Spatial heterogeneity in tumor perfusion measured with functional computed tomography at 0.05 microliter resolution. *Cancer Res* 54(23):6032–6036.